Journal of Molecular Structure 1102 (2015) 170–185

Contents lists available at ScienceDirect

Journal of Molecular Structure

journal homepage: http://www.elsevier.com/locate/molstruc

An environmentally friendly method to remove and utilize the highly toxic strychnine in other products based on proton-transfer complexation

Abdel Majid A. Adam [a, *], Moamen S. Refat [a, b], Hosam A. Saad [a, c], Mohamed S. Hegab [d, e]

[a] Department of Chemistry, Faculty of Science, Taif University, Al-Haweiah, P.O. Box 888, 21974 Taif, Saudi Arabia
[b] Department of Chemistry, Faculty of Science, Port Said University, Port Said, Egypt
[c] Department of Chemistry, Faculty of Science, Zagazig University, Zagazig, Egypt
[d] Deanship of the Preparatory Year, Taif University, Al-Haweiah, P.O. Box 888, 21974 Taif, Saudi Arabia
[e] Department of Chemistry, Faculty of Science, Ain Shams University, P.O. Box 11566, Cairo, Egypt

ARTICLE INFO

Article history:
Received 17 May 2015
Received in revised form
26 August 2015
Accepted 29 August 2015
Available online 3 September 2015

Keywords:
Strychnine
Proton-transfer
Nanoporous carbon
SEM
TEM

ABSTRACT

The study of toxic and carcinogenic substances represents one of the most demanding areas in human safety, due to their repercussions for public health. There is great motivation to remove and utilize these substances in other products instead of leaving them contaminate the environment. One potentially toxic compound for humans is strychnine (Sy). In the present study, we attempted to establish a quick, simple, direct and efficient method to remove and utilize discarded Sy in other products based on proton-transfer complexation. First, Sy was reacted with the acido organic acceptors PA, DNBA and CLA. Then, the resultant salts were direct carbonized into carbon materials. Also, this study provides an insight into the structure and morphology of the obtained products by a range of physicochemical techniques, such as UV–visible, IR, ^{1}H NMR and ^{13}C NMR spectroscopies; XRD; SEM; TEM; and elemental and thermal analyses. Interestingly, the complexation of Sy with the PA or DNBA acceptor leads to a porous carbon material, while its complexation with CLA acceptor forms non-porous carbon product.

1. Introduction

Strychnine (Sy), chemically strychnidin-10-on, the structure of which is shown in Fig. 1, is a monoterpene indole alkaloid found as a white odorless and bitter crystalline powder. The primary natural source of Sy is the seeds of *Strychnos nux-vomica* L. (Loganiaceae), a tree grown extensively in China and southern Asian countries [1,2]. It is found together with brucine and other indole alkaloids in various plants of the strychnine family [2]. It has been effectively used in traditional Chinese medicine to treat central nervous system diseases and to alleviate allergic symptoms, joint pain and traumatic pain [3]. Sy when ingested could stimulate the central nervous system and make the sensory organs more sensitive [4]. So at low doses (such as at 10 mg daily dose) it is often used to treat nervous diseases and vomiting as well as arthritic and traumatic pains [5]. However, Sy is highly toxic to humans and most domestic animals and the margin between therapeutic and toxic doses is very narrow as it was reported to be fatal to man at doses of 30–90 mg [6]. It has been demonstrated that a high of the Sy can induce convulsions of the central nervous system and death through respiratory or spinal paralysis or cardiac arrest [7]. Nowadays, Sy is no longer used as a therapeutic drug and its availability to the public is controlled by legislations in various jurisdictions, but it is still in limited use as a rodenticide, pesticide, fungicide and an adulterant in street drugs [8,9]. Porous and nanostructured carbon materials have attracted much attention because of their versatile applications in catalysis, sensors, electronic devices, electrodes, gas and liquid separation, and memory storage [10–12]. Activated porous carbons have received significant attention as potential hydrogen storage media due to their low density, high surface area, large pore volume, god chemical stability, and high storage capacity [13]. For several years, we have investigated the synthesis, characterization and application of various charge-transfer (CT) and proton-transfer (PT) interactions [14–28]. As part of our continuing interest in this field, in this work, we originally report a method to remove and utilize discarded Sy in

* Corresponding author.
E-mail address: majidadam@yahoo.com (A.M.A. Adam).

http://dx.doi.org/10.1016/j.molstruc.2015.08.065
0022-2860/

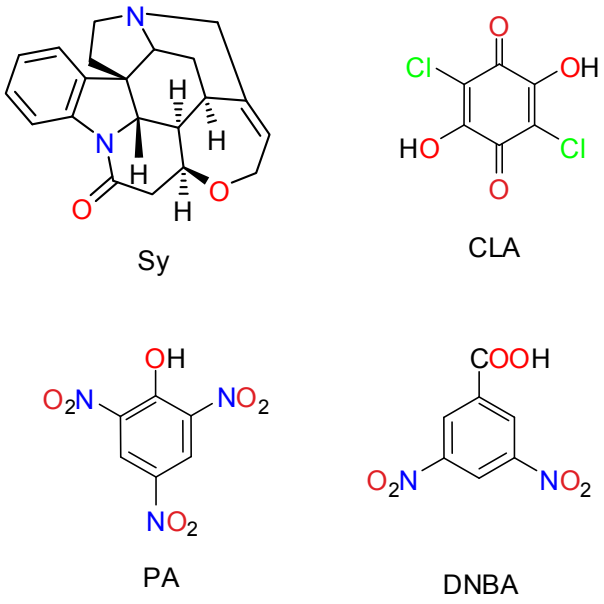

Fig. 1. The structure of strychnine (Sy) and organic acceptors.

other products as porous carbon material. First, Sy was directly reacted with acido organic acceptors (PA, DNBA and CLA) to form proton-transfer salts. Then, the resultant salts were direct carbonized at 400 °C into carbon materials. The obtained products were characterized by elemental, thermal and spectroscopic data (UV–Vis, IR, ^{1}H and ^{13}C NMR). Their morphology and nanometry were observed and differentiated using X-ray diffraction (XRD), scanning electron microscopy (SEM) and transmission electron microscopy (TEM) techniques.

2. Experiment and calculations

2.1. Chemicals and solutions

All of the chemicals used were of analytical grade and were used as purchased. Strychnine (Sy; $C_{21}H_{22}N_2O_2$, 334.42) was supplied by Sigma–Aldrich Chemical Co. (USA). The organic acceptors picric acid (PA; $C_6H_3N_3O_7$; 229.10), 3,5-dinitrobenzoic acid (DNBA; $C_7H_4O_6N_2$; 212.12), and chloranilic acid (CLA; $C_6H_2Cl_2O_4$; 208.98) were purchased from Merck (Darmstadt, Germany) and were used without modification. HPLC-grade methanol and chloroform were also purchased from Merck. Standard stock solutions at a concentration of 5.0×10^{-3} M were freshly prepared prior to each series of measurements by dissolving precisely weighed quantities in a 100 mL volumetric flask. The stock solutions were protected from light. Solutions for spectroscopic measurements were prepared by mixing appropriate volumes of the Sy and acceptor stock solutions with the solvent immediately before recording the spectra.

2.2. Characterization methods

2.2.1. CHN analysis

To ascertain the constituents, purity and compositions of the synthesized salts, the carbon, hydrogen and nitrogen contents were analyzed with a Perkin–Elmer 2400 series CHN microanalyzer (USA).

2.2.2. UV–Vis spectra

The UV–Vis spectra were recorded over a wavelength range of 200–800 nm using a Perkin–Elmer Lambda 25 UV/Vis double-beam spectrophotometer with quartz cells. The path length of the cells was 1.0 cm.

2.2.3. IR spectra

The infrared (IR) spectra of the solid products (as KBr discs) were acquired at room temperature using a Shimadzu FT-IR spectrophotometer (Japan) over the range of 4000–400 cm^{-1}.

2.2.4. ^{1}H and ^{13}C spectra

^{1}H and ^{13}C NMR spectra were collected on a Bruker DRX-250 spectrometer operating at 600 MHz. The measurements were performed at ambient temperature using DMSO-d_6 (dimethylsulfoxide, d_6) as the solvent and TMS (tetramethylsilane) as the internal reference.

2.2.5. Thermal analysis

Thermogravimetric (TG) analysis was performed using a Shimadzu TGA–50H thermal analyzer (Japan) with standard platinum TG pans. The measurements were conducted at a constant heating rate of 10 °C/min over the temperature range of 25–600 °C in a nitrogen atmosphere using alumina powder as the reference material.

2.2.6. XRD analysis

The X-ray diffraction (XRD) profiles were obtained using a PANalytical X'Pert PRO X-ray powder diffractometer. The instrument was equipped with a Ge(III) secondary monochromator, and Cu $K\alpha_1$ was employed as the radiation source, with a wavelength of 0.154056 nm. The samples were scanned with 2θ between 5° and 90°.

2.2.7. SEM analysis

The microstructure and morphology were analyzed by a scanning electron microscope (SEM, Quanta FEG 250 instrument). The instrument was operated at an accelerating voltage of 20 kV.

2.2.8. TEM analysis

The particle size was analyzed by transmission electron microscope (TEM, JEOL JEM-1200 EX II, Japan). The instrument was operated at an accelerating voltage of 60–70 kV.

2.3. Preparation of materials

2.3.1. Preparation of the salts

A simple synthetic protocol has been used for the preparation of PT complexes of Sy donor. A typical procedure for the preparation is briefly described as follows. First, 2 mmol of Sy in chloroform (20 ml) was added to 20 ml of a solution containing 2 mmol of the acceptor (either PA, DNBA or CLA) in the methanol solvent. The resulting mixture was stirred at room temperature for approximately half an hour, where the resulting precipitation were isolated as yellow canary, white and reddish-brown powder for Sy–PA, Sy–DNBA and Sy–CLA salts, respectively. The formed products were isolated, filtered and further purified using methanol-chloroform solvent and a recrystallization process to obtain the pure products. The products were then collected and dried *in vacuo* for 48 h. The products were characterized by spectroscopy (UV–Vis, IR, ^{1}H and ^{13}C NMR) as well as elemental and thermal analyses. The excellent agreement between the experimental and calculated values of C, H and N indicates that the obtained products are free of impurities. The stoichiometry of the Sy interaction with the acceptors was found to have a 1:1 ratio.

2.3.1.1. Sy free. white powder; IR (KBr, cm^{-1}): υ_{max} 3050–2950

ν(C–H), 1697 ν_{as} (C=O), 1672 ν_s(C=O), 1670–1479 ν(C=C), 1385 ν_{as}(C–N). ^{1}H NMR (DMSO-d_6, 600 MHz): δ = 1.20 (m, 1H, $C_{(13)}H$ proton), 1.40 (m, 1H, $C_{(15)}H_a$ proton), 1.82 (m, 2H, $C_{(17)}$ H_a, H_b protons), 1.90 (m, 1H, $C_{(15)}$ H_b proton), 2.30 (dd, 1H, $C_{(11)}$ H_b proton), 2.65 (d, 1H, $C_{(20)}$ H_a proton), 2.85 (m, 1H, $C_{(18)}$ H_b proton), 3.17–3.95 (m, 6H, $C_{(11)}H_a$, $C_{(14)}$ H, $C_{(18)}$ H_a, $C_{(20)}$ H_b, $C_{(8)}$ H and $C_{(16)}$ H protons), 4.13–4.32 (m, 4H, $C_{(23)}$ H_a, H_b, $C_{(12)}$ H), 5.84 (dd, 1H, $C_{(22)}$ H protons), 7.09 (dd, 1H, $C_{(2)}$ H proton), 7.15 (d, 1H, $C_{(1)}$ H proton), 7.20 (dd, 1H, $C_{(3)}$ H proton), 8.10 (d, 1H, $C_{(4)}$ H proton). ^{13}C NMR (DMSO-d_6, 150 MHz): δ = 26.71, 31.45, 42.33, 42.74, 48.07, 50.19, 52.53, 59.96, 60.04, 64.46, 77.44 (*sp^3 carbons*, *CH*, *CH_2*), 116.0, 122.1, 124.0, 127.0, 128.3, 132.6, 140.4, 142.0, 169.1 (*sp^2 carbons* Ar–C, C=C and C=O). Anal. Calcd for $C_{21}H_{22}N_2O_2$ (334.42), C, 75.35; H, 6.58; N, 8.37; Found, C, 75.15; H, 6.66; N, 8.20. The structure of the Sy with its corresponding atom numbering scheme is shown in Fig. 2.

2.3.1.2. Free acceptors. (a) PA; ^{1}H NMR (DMSO-d_6, 600 MHz): δ = 8.59 (s, 2H, picric acid C_3, C_5 protons), 9.94 (s, 1H, picric acid OH protons). ^{13}C NMR (DMSO-d_6, 150 MHz): δ = 126.5, 140.8, 142.6, 156.3 (*sp^2 carbons* Ar–C). *(b) DNBA*; ^{1}H NMR (DMSO-d_6, 600 MHz): δ = 9.11 (s, 2H, dinitrobenzoic acid $C_{(2,6)}$ H protons), 9.18 (s, 1H, dinitrobenzoic acid $C_{(4)}$ H proton), 12.10 (s, 1H, dinitrobenzoic acid COO*H* proton). ^{13}C NMR (DMSO-d_6, 150 MHz): δ = 123.3, 130.0, 134.3, 148.7, 163.9 (*sp^2 carbons* Ar–C and C=O). *(c) CLA*; ^{1}H NMR (DMSO-d_6, 600 MHz): δ = 10.68 (s, 1H, chloranilic acid OH proton). ^{13}C NMR (DMSO-d_6, 150 MHz): δ = 124.5, 163.9, 168.2 (*sp^2 carbons* Ar–C, C=C and 2C=O).

2.3.1.3. Sy–PA complex. Yellow canary powder; IR (KBr, cm^{-1}): υ_{max} 3439 υ($^+$N–H ··· O$^-$), 2989, 2945 ν(C–H), 2855, 2756 υ(N–H ··· O), 1657 ν_{as} (C=O), 1622 ν_s(C=O), 1565, 1480 ν(C=C), 1325 ν_{as}(C–N). ^{1}H NMR (DMSO-d_6, 600 MHz): δ = 1.44 (m, 1H, $C_{(13)}$ H proton), 1.61 (m, 1H, $C_{(15)}$ H_a proton), 1.95 (m, 2H, $C_{(17)}$ H_a, H_b protons), 2.16 (m, 1H, $C_{(15)}$ H_b proton), 2.68 (dd, 1H, $C_{(11)}$ H_b proton), 2.95 (d, 1H, $C_{(20)}$ H_a proton), 3.52 (m, 1H, $C_{(18)}$ H_b proton), 4.07–4.17 (m, 6H, $C_{(11)}$ H_a, $C_{(14)}$ H, $C_{(18)}$ H_a, $C_{(20)}$ H_b, $C_{(8)}$ H and $C_{(16)}$ H protons), 4.43–4.50 (m, 4H, $C_{(23)}$ H_a, H_b, $C_{(12)}$ H, $C_{(22)}$ H protons), 6.45 (s, 1H, $N^+_{(19)}$ H), 7.14 (dd, 1H, $C_{(2)}H$ proton), 7.29 (d, 1H, $C_{(1)}$ H proton), 7.43 (dd, 1H, $C_{(3)}$ H proton), 7.93 (d, 1H, $C_{(4)}$ H proton), 8.58 (s, 2H, picric acid protons). ^{13}C NMR (DMSO-d_6, 150 MHz): δ = 24.79, 30.11, 40.50, 41.20, 47.50, 51.41, 51.82, 52.22, 59.00, 62.11, 63.62, 77.50 (*sp^3 carbons*, *CH*, *CH_2*), 115.7, 118.3, 122.1, 125.6, 125.8, 129.0, 129.30, 130.0, 135.3, 140.4, 142.3, 161.2, 169.3 (*sp^2 carbons* Ar–C, C=C and C=O). Anal. Calcd for $C_{27}H_{25}N_5O_9$ (563.52), C, 57.50; H, 4.44; N, 12.42; Found, C, 57.46; H, 4.48; N, 12.40.

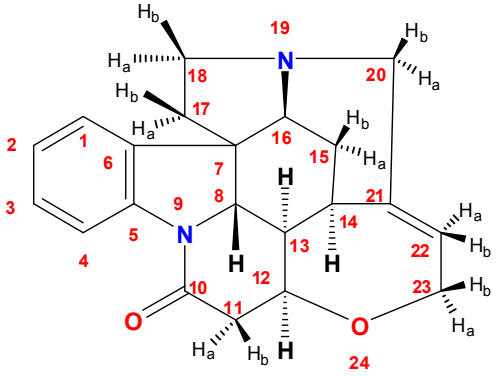

Fig. 2. The structure of Sy with atom numbering.

2.3.1.4. Sy–DNBA complex. white powder; IR (KBr, cm^{-1}): υ_{max} 3430 υ($^+$N–H ··· O$^-$), 2962, 2927 ν(C–H), 2883, 2851 υ(N–H ··· O), 1677 ν_{as} (C=O), 1619 ν_s(C=O), 1543, 1470 ν(C=C), 1349 ν_{as}(C–N). ^{1}H NMR (DMSO-d_6, 600 MHz): δ = 1.43 (m, 1H, $C_{(13)}$ H proton), 1.46 (m, 1H, $C_{(15)}$ H_a proton), 1.59 (m, 2H, $C_{(17)}$ H_a, H_b protons), 2.15 (m, 1H, $C_{(15)}$ H_b proton), 2.66 (dd, 1H, $C_{(11)}$ H_b proton), 2.94 (d, 1H, $C_{(20)}$ H_a proton), 3.32 (m, 1H, $C_{(18)}$ H_b proton), 4.06–4.18 (m, 6H, $C_{(11)}$ H_a, $C_{(14)}$ H, $C_{(18)}$ H_a, $C_{(20)}$ H_b, $C_{(8)}$ H and $C_{(16)}$ H protons), 4.45–4.48 (m, 4H, $C_{(23)}$ H_a, H_b, $C_{(12)}$ H, $C_{(22)}$ H protons), 6.34 (s, 1H, $N^+_{(19)}$H), 7.14 (dd, 1H, $C_{(2)}$ H proton), 7.28 (d, 1H, $C_{(1)}$ H proton), 7.45 (dd, 1H, $C_{(3)}$ H proton), 7.93 (d, 1H, $C_{(4)}$ H proton), 8.92 (s, 2H, dinitrobenzoic acid $C_{(2,6)}$ H protons), 8.95 (s, 1H, dinitrobenzoic acid $C_{(4)}$ H proton). ^{13}C NMR (DMSO-d_6, 150 MHz): δ = 24.52, 29.87, 40.55, 41.18, 47.50, 51.40, 51.82, 52.22, 58.67, 60.35, 63.62, 77.50 (*sp^3 carbons*, *CH*, *CH_2*), 115.2, 120.8, 122.9, 124.2, 128.7, 129.1, 129.3, 132.0, 134.0, 137.6, 141.8, 148.1, 164.8, 168.8 (*sp^2 carbons* Ar–C, C=C and 2C=O). Anal. Calcd for $C_{28}H_{26}N_4O_8$ (546.54), C, 61.48; H, 4.76; N, 10.25; Found, C, 61.53; H, 4.81; N, 10.07.

2.3.1.5. Sy–CLA complex. reddish-brown powder; IR (KBr, cm^{-1}): υ_{max} 3438 υ($^+$N–H ··· O$^-$), 2962 ν(C–H), 1681 ν_{as} (C=O), 1617 ν_s(C=O), 1572 ν(C=C), 1317 ν_{as}(C–N). ^{1}H NMR (DMSO-d_6, 600 MHz): δ = 1.40 (m, 1H, $C_{(13)}$ H proton), 1.49 (m, 1H, $C_{(15)}$ H_a proton), 1.57 (m, 2H, $C_{(17)}$ H_a, H_b protons), 2.13 (m, 1H, $C_{(15)}$ H_b proton), 2.67 (dd, 1H, $C_{(11)}$ H_b proton), 2.95 (d, 1H, $C_{(20)}$ H_a proton), 3.32 (m, 1H, $C_{(18)}$ H_b proton), 4.07–4.20 (m, 6H, $C_{(11)}$ H_a, $C_{(14)}$ H, $C_{(18)}$ H_a, $C_{(20)}$ H_b, $C_{(8)}$ H and $C_{(16)}$ H protons), 4.44–4.50 (m, 4H, $C_{(23)}$ H_a, H_b, $C_{(12)}$ H, $C_{(22)}$ H protons), 6.36 (s, 1H, $N^+_{(19)}$ H), 7.14 (dd, 1H, $C_{(2)}$ H proton), 7.28 (d, 1H, $C_{(1)}$ H proton), 7.45 (dd, 1H, $C_{(3)}$ H proton), 7.93 (d, 1H, $C_{(4)}$ H proton), 8.72 (s, 1H, chloranilic acid OH proton). ^{13}C NMR (DMSO-d_6, 150 MHz): δ = 24.37, 29.67, 39.51, 42.54, 47.90, 50.14, 51.88, 53.52, 58.66, 61.89, 64.12, 76.84 (*sp^3 carbons*, *CH*, *CH_2*), 115.5, 121.1, 122.5, 124.5, 127.2, 129.3, 129.7, 133.8, 135.1, 136.9, 142.9, 146.4, 163.4, 164.1, 167.4 (*sp^2 carbons* Ar–C, C=C and 3C=O). Anal. Calcd for $C_{27}H_{24}Cl_2N_2O_6$ (543.40), C, 59.62; H, 4.42; N, 5.15; Found, C, 59.66; H, 4.23; N, 5.11.

2.3.2. Preparation of carbon materials

In a typical process, the salts were dried at 110 °C overnight, then carbonized into carbon material in a furnace at 400 °C under N_2 flow for 1.0 h. The as-prepared non-activated carbon product was ground into powder with a particle size of 2–3 mm and characterized by XRD, SEM and TEM techniques.

2.4. Calculation details

2.4.1. Calculations of the spectroscopic parameters

2.4.1.1. Calculation of the formation constant and molar extinction coefficient. The formation constant (K) and the molar extinction coefficient (ε) were determined spectrophotometrically using the 1:1 Benesi–Hildebrand equation (Eq. (1)) [29]. C_a and C_d are the initial concentrations of the acceptor and donor, respectively, and A is the absorbance of the CT band. By plotting the $(C_a\,C_d)/A$ values for the 1:1 CT complex as a function of the corresponding $(C_a + C_d)$ values, a straight line is obtained with a slope of $1/\varepsilon$ and an intercept at $1/K\varepsilon$.

$$(C_aC_d)/A = 1/K\varepsilon + (C_a + C_d)/\varepsilon \quad (1)$$

2.4.1.2. Calculation of the energy value. The energy values (E_{CT}) of the n → π* and π → π* interactions between the donor and the acceptor were calculated using the equation derived by Briegleb (Eq. (2)) [30], where λ_{CT} and ν_{CT} are the wavelength and wavenumber of the complexation band of the formed complex,

respectively.

$$E_{CT} = (h\nu_{CT}) = 1243.667/\lambda_{CT}(\text{nm}) \quad (2)$$

2.4.1.3. Calculation of the oscillator strength. The oscillator strength (f) is a dimensionless quantity used to express the transition probability of a band. From the absorption spectra, f can be obtained using the approximate formula given in Eq. (3) [31]. $\int \varepsilon_{CT}\, d\nu$ is the area under the curve of the extinction coefficient of the absorption band in question plotted as a function of the frequency. To a first approximation, f can be calculated using Eq. (4). ε_{CT} is the maximum extinction coefficient of the CT band, and $\nu_{½}$ is the full-width at half-maximum (FWHM) in cm^{-1}.

$$f = 4.319 \times 10^{-9} \int \varepsilon_{CT} d\nu \quad (3)$$

$$f = 4.319 \times 10^{-9} \varepsilon_{CT} \nu_{½} \quad (4)$$

2.4.1.4. Calculation of the transition dipole moment. The transition dipole moments (μ) are calculated using Eq. (5) [32], where ν_{max} is the full width of the CT band at maximum in cm^{-1}. The transition dipole moment (μ) can be employed to determine whether a particular transition is allowed. The transition from a bonding π orbital to an antibonding π^* orbital is allowed because the integral that defines the transition dipole moment is nonzero.

$$\mu\ (\text{Debye}) = 0.0958\ [\varepsilon_{CT}\nu_{½}/\nu_{max}]^{½} \quad (5)$$

2.4.1.5. Calculation of the standard free energy change. The values of the standard free energy change (ΔG°) were calculated from the formation constants using Eq. (6) [33]. ΔG° is the standard free energy change of the complexes (J mol^{-1}), R is the universal gas constant (8.314 J mol^{-1} K^{-1}), T is the absolute temperature in Kelvin, and K is the formation constant of the complex (L mol^{-1}) at room temperature.

$$\Delta G^\circ = -2.303RT \log K_{CT} \quad (6)$$

2.4.2. Calculation of the particle sizes

The particle size of the complexes was estimated from their XRD patterns based on the highest intensity line using the well-known Debye–Scherrer formula, given in the following equation [34]:

$$D = 0.94\lambda/\beta\cos\theta \quad (7)$$

where D is the apparent particle size of the grains in nanometers, 0.94 is the Scherrer constant (for a Cu grid), λ is the wavelength of the incident X-ray (Cu Kα; 0.15406 nm), θ is the position of the selected diffraction peak (i.e., the Bragg diffraction angle), and β is

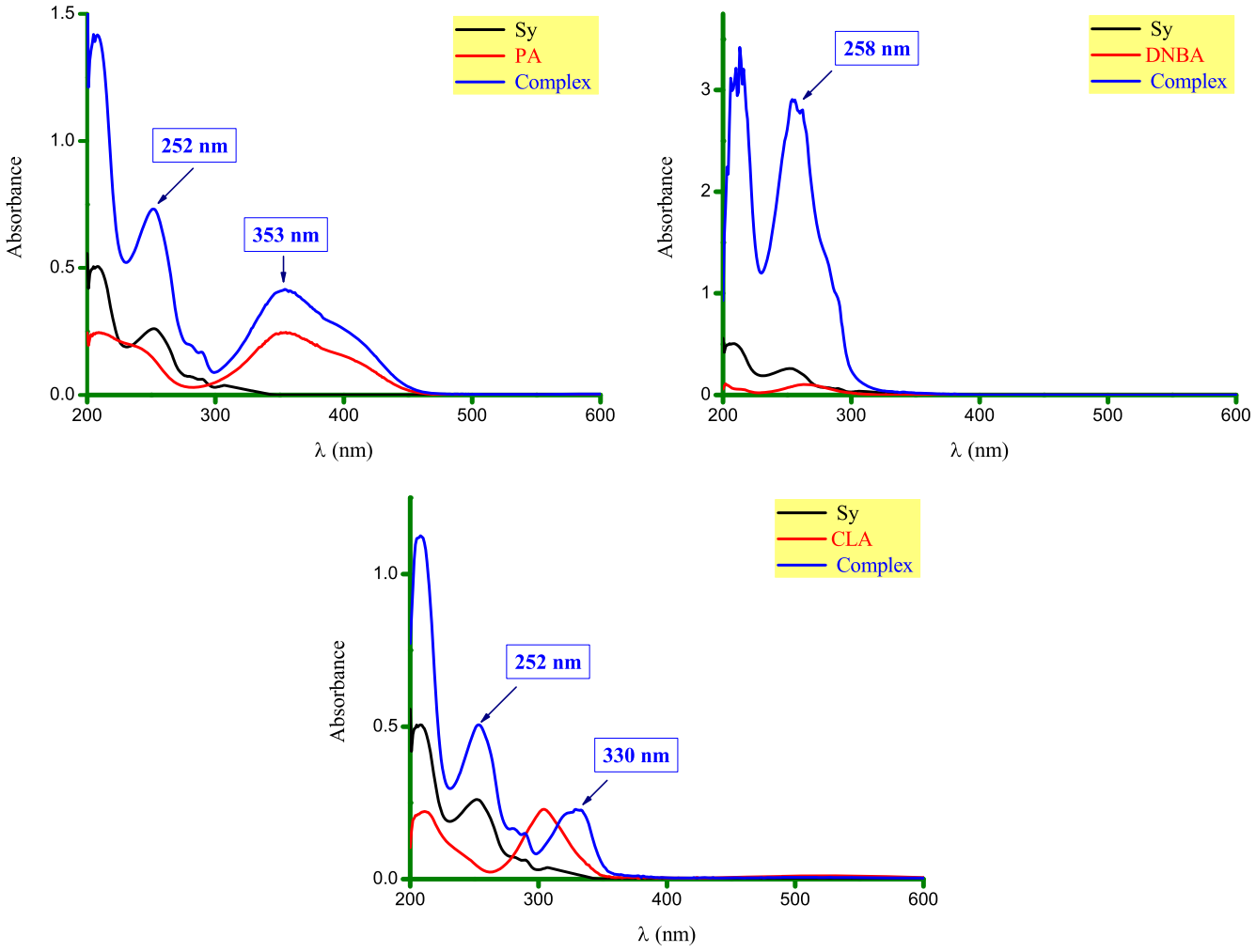

Fig. 3. Electronic absorption spectra of the Sy complexes with PA, DNBA and CLA acceptors.

the FWHM of the characteristic X-ray diffraction peak (with additional peak broadening) in radians.

3. Results and discussion

3.1. Spectral properties

3.1.1. UV–visible measurements

Sy (5.0×10^{-4} M) was mixed with each acceptor solution (5.0×10^{-4} M), and the reaction was allowed to proceed at room temperature. The UV–visible spectrum of each reaction mixture was then recorded against a reagent blank solution. Fig. 3 displays the UV–visible absorption spectra of the Sy and acceptors, along with the spectra of the prepared complexes. This figure indicates a remarkable change in the UV–Vis spectrum of the Sy upon the addition of acceptor to the solution. The absorption spectrum of Sy has two λ_{max} at 207 nm and 252 nm, while PA acceptor displays two measurable absorption band λ_{max} at 207 nm and 353 nm. When Sy and PA are mixed together, these characteristic bands increases strongly in intensity and becomes more broad. These changes provided strong evidence of interaction between Sy and PA and the formation of PT complex. Interestingly, on mixing the solutions of the Sy and DNBA, a very strong broad band was observed at 258 nm that correspond to the PT interaction. The spectrum of the Sy–CLA complex was characterized by a new absorption band appeared at a longer wavelength (330 nm) in regions where Sy has no measurable absorption. This new strong broadening band at longer wavelengths are presumably caused by the Sy–CLA interaction and is indicative of the formation of a PT complex.

The stoichiometry of the Sy–acceptor interactions in solution was obtained from the spectrophotometric titrations by determining the conventional molar ratio according to previously published protocols [35]. The electronic spectra of the Sy–acceptor systems were recorded at varying acceptor concentrations and a constant Sy concentration. The composition of the complexes was determined graphically by plotting the absorbance on the ordinate against the volume of the acceptor (in mL) on the abscissa. Representative spectrophotometric titration plots based on the characterized absorption bands are shown in Fig. 4. The results show that the greatest interaction between Sy and each acceptor occurred at a donor: acceptor ratio of 1:1, indicating that 1:1 complexes were formed. These stoichiometric values are consistent with the data obtained by the elemental analysis of the solid-state complexes.

3.1.2. The spectroscopic data

The 1:1 Benesi–Hildebrand equation was used to determine the spectroscopic parameters of the synthesized complexes. Fig. 5 shows a representative 1:1 Benesi–Hildebrand plot of the Sy complexes. The values of both K and ε have been determined from these data and, along with the other spectroscopic parameters (e.g., f, μ, E_{CT} and ΔG°), are provided in Table 1. Fig. 5 reveals that the

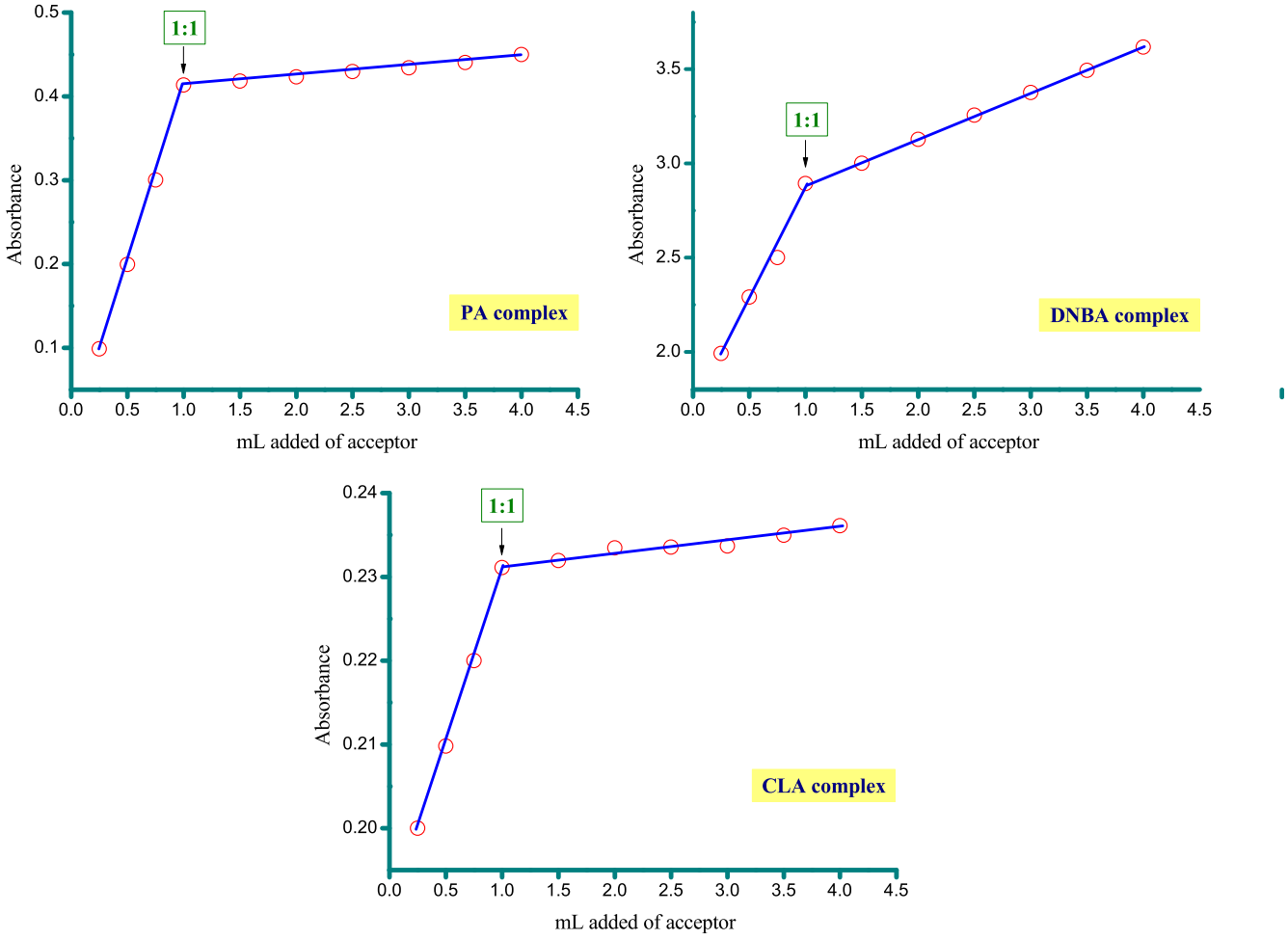

Fig. 4. Spectrophotometric titration curves for the Sy complexes with PA, DNBA and CLA acceptors.

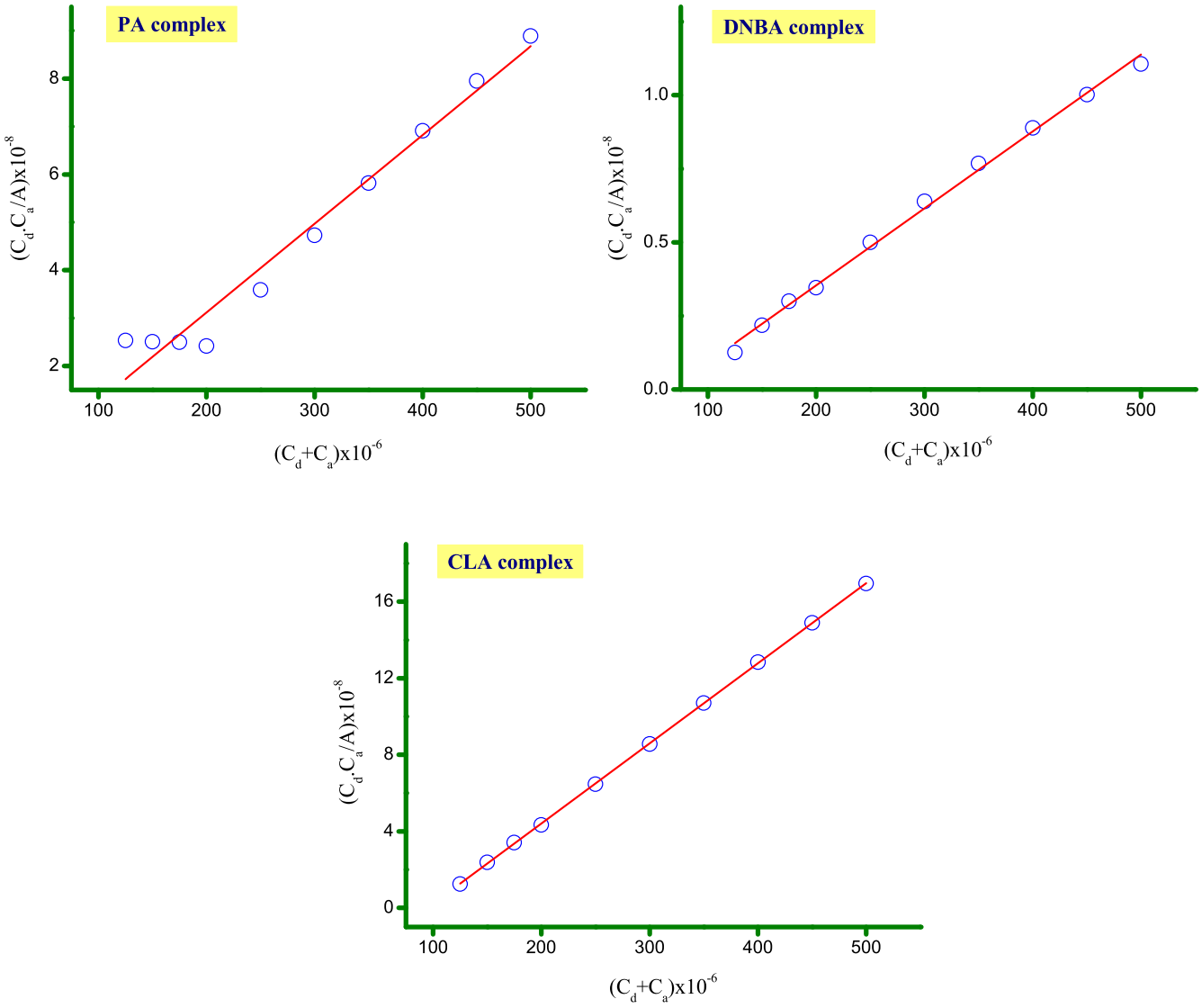

Fig. 5. The 1:1 Benesi–Hildebrand plots of the Sy complexes with PA, DNBA and CLA acceptors.

correlation coefficient (r) of the straight lines is > 0.99. The complex containing the DNBA acceptor shows a higher K value than the other complexes. This high value of K reflects the relatively high electron acceptance ability of DNBA and suggests that the Sy–DNBA complex is strongly bound and highly stable. The stability of the complexes decreases in the following order: Sy–PA > Sy–DNBA > Sy–CLA. All the ΔG° values are negative, indicating that the complexation between Sy and the acceptors is exothermic and spontaneous. The ΔG° values of the complexes for the different acceptors are ordered as follows: PA > DNBA > CLA. We note that this ordering is consistent with the stability of the Sy complexes. Linear correlations were observed between several pairs of spectroscopic parameters (Fig. 6). For example, a very strong linear correlation ($r = 0.9999$) exists between the oscillator strength (f) and the dipole moment (μ) in solution. This finding indicates that the oscillator strength values of the complexes in solution increased as their dipole moment values increased. A strong linear relationship ($r = 0.9865$) was obtained between f and

Table 1
Spectral properties of the Sy complexes.

Property	Complex		
	Sy–PA	Sy–DNBA	Sy–CLA
λ_{max} (nm)	353	258	330
Formation constant; K ($Lmol^{-1}$)	31×10^5	15.5×10^5	10.5×10^5
Extinction coefficient; ε_{max} ($Lmol^{-1}$ cm^{-1})	54×10^4	385×10^4	24×10^4
Energy value; E_{CT} (eV)	3.52	4.82	3.77
Oscillator strength; f	2.32	33.22	2.58
Dipole moment; μ	1.32	4.26	1.34
Standard free energy change; ΔG° (kJ mol^{-1})	-3.71×10^4	-3.53×10^4	-3.44×10^4

extinction coefficient (ε_{max}). In addition, a strong linear correlation ($r = 0.9394$) is observed between the f and the energy value (E_{CT}). Finally, a strong linear relationship ($r = 0.9752$) is also observed between the standard free energy change (ΔG°) and the formation constant (K). The values of ΔG° become more negative as the formation constant for the molecular complex increases.

3.1.3. IR measurements

The molecular structure of Sy consists of seven condensed rings with six asymmetric centers. On account of reducing the strain in the oligocyclic ring system, the rings are non-planar [36]. In addition there is a planar phenyl ring. The ring system contains two ternary nitrogen atoms in (C–N) groups; the nitrogen of the tetrahydropyridoindol nucleus which is bonded to a carbonyl group and the nitrogen of the octahydroethanoindole nucleus, and all of them are sp^3 hybridized nitrogens. They differ from each other in basicity, mainly due to resonance, which decreases the basicity and the steric hindrance. The least basic one is the nitrogen of the tetrahydropyridoindol nucleus, due to the resonance effect of the amide nitrogen with the adjacent carbonyl group leading to partial positive charge on nitrogen atom for somewhat as shown in Fig. 7. The most basic one is the nitrogen of the octahydroethanoindole nucleus, due to the absent of adjacent resonance and the electron repelling effect of the three attached alkyl groups along with the less steric hindrance around its lone pair of electron. The last is the nitrogen atom most expected to be able to accept the acidic proton of acceptors. The IR spectrum of the free Sy was characterized by principal absorption peaks at 3050-2950 cm^{-1} for C–H symmetric and asymmetric stretching, 1697 and 1672 cm^{-1} for ν(C=O) of the amide group, 1670-1479 cm^{-1} for ν(C=C), and 1465 cm^{-1} for ν_{as}(C–N) [37]. The IR spectra of the Sy–PA and Sy–DNBA complexes are characterized by a group of medium bands at 2855 and 2756 cm^{-1} for PA complex, and at 2883 and 2851 cm^{-1} for DNBA complex (Fig. 8). These new broadened bands are attributed to ν($^{+}$N–H) and confirm the migration of the PA or DNBA proton towards the nitrogen of the Sy octahydroethanoindole nucleus to form an intermolecular H-bonded ion pair ($^{+}$N–H ··· O^{-}). Generally,

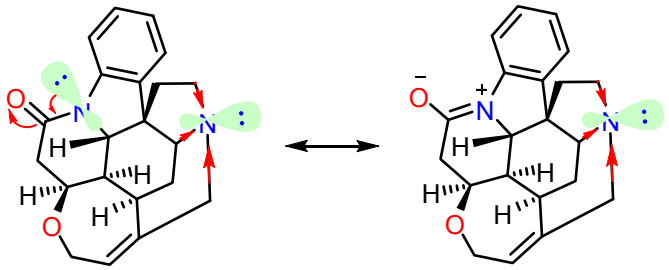

Fig. 7. Resonating structures of the amide carbonyl group.

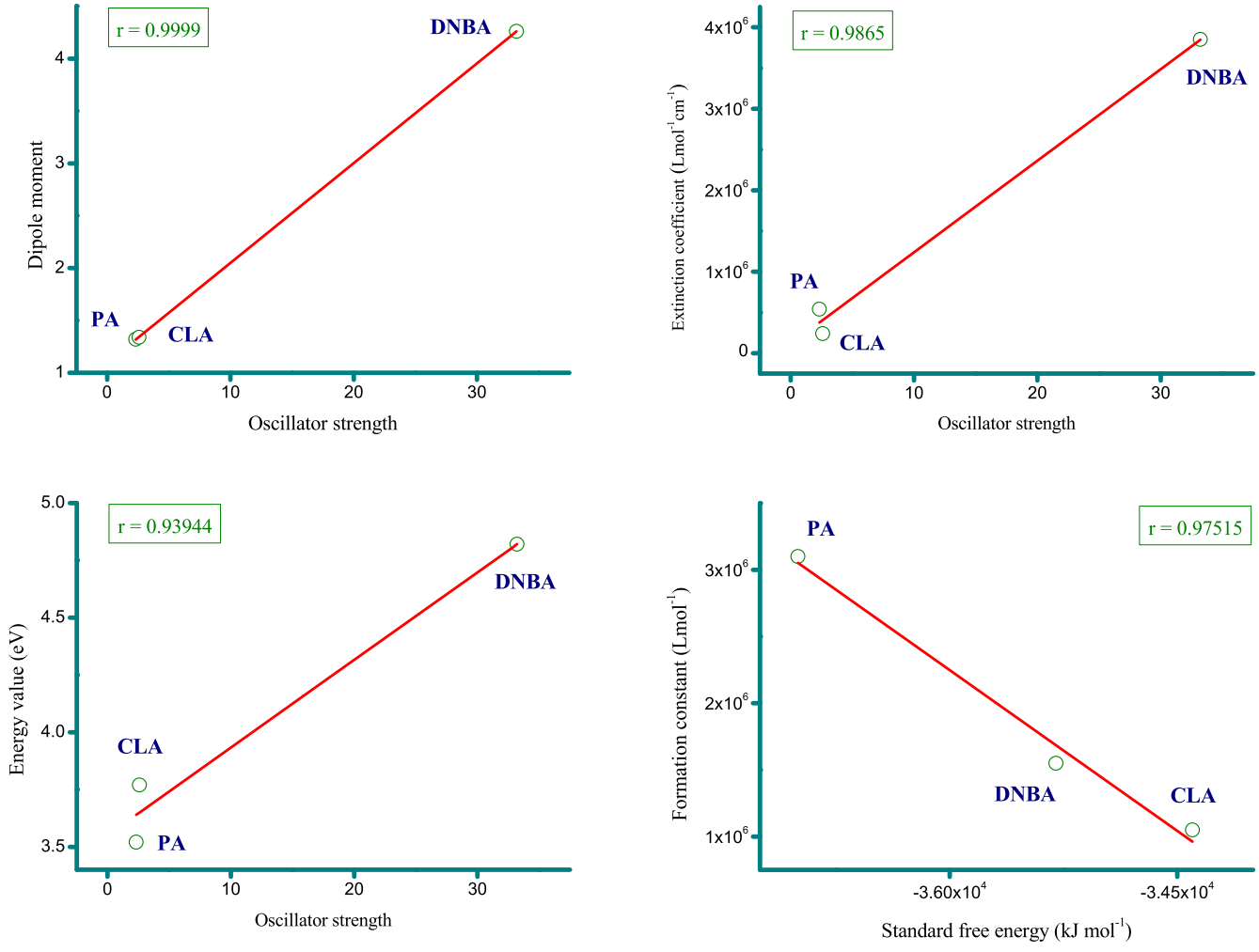

Fig. 6. Linear correlations of some spectroscopic parameters.

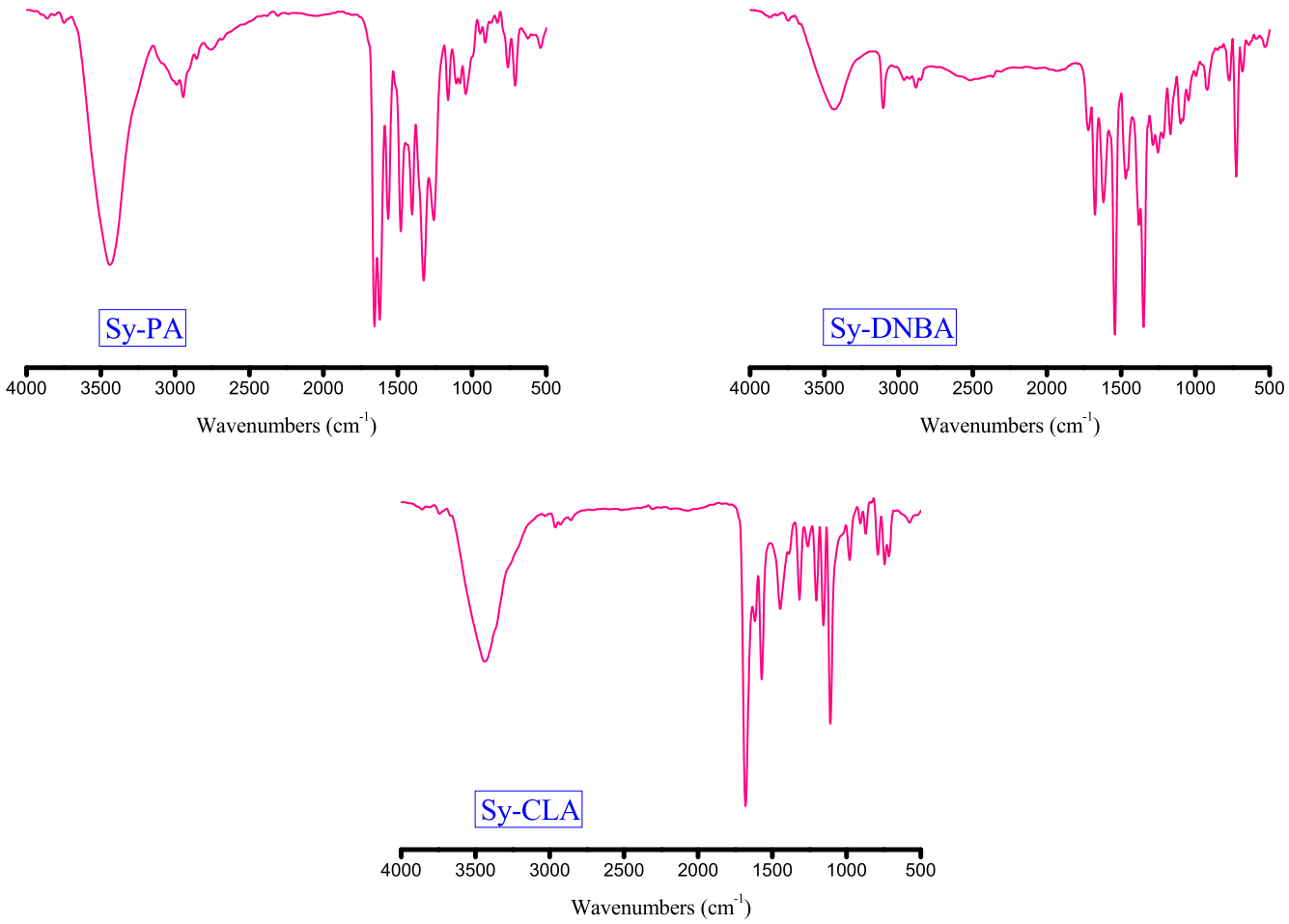

Fig. 8. IR spectra of the Sy complexes.

the intermolecular hydrogen bonding that exists in a PT complex is expected to be found at approximately 3400 cm^{-1} [38]. The bands observed at approximately 3439 cm^{-1} for the PA complex, at 3430 cm^{-1} for the DNBA complex, and at 3438 cm^{-1} for the CLA complex are a result of the stretching vibration of ($^{+}$N–H ··· O^{-}). Additionally, the characteristic band observed at 1385 cm^{-1} that results from the ν(C–N) vibration of the free Sy shifts to ~1325 cm^{-1} in Sy–PA, ~1349 cm^{-1} in Sy–DNBA, and ~1317 cm^{-1} in

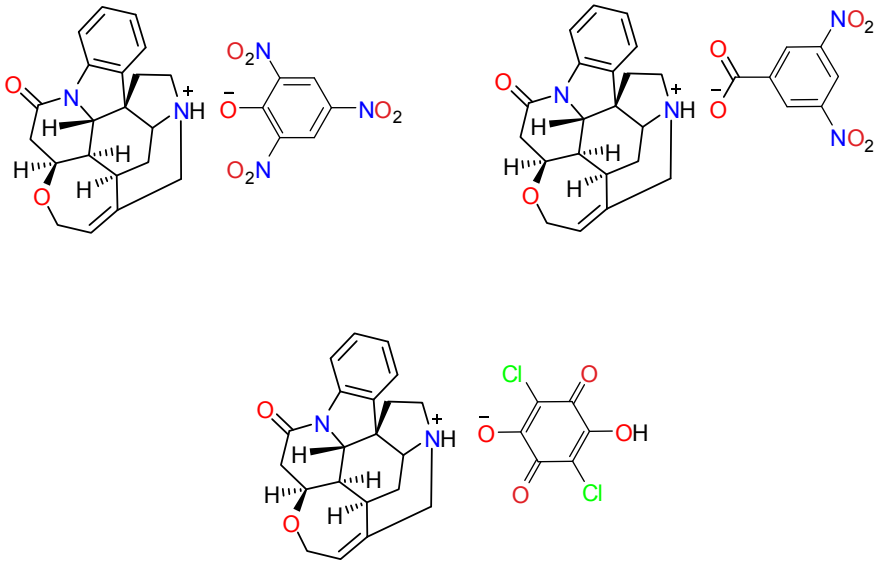

Fig. 9. Proposed structural formula of the Sy–PA and Sy–DNBA and Sy–CLA proton-transfer complex.

Table 2
Thermal decomposition data for the synthesized Sy complexes.

Compound	Stages	TG range (°C)	TG% mass loss		Lost species
			Found	Calculated	
Sy–PA	I	190–350	40.84	40.67	PA
	II	350–600	50.32	50.81	$C_{17}H_{22}N_2O_2$
	Residue	–	8.40	8.52	4C
Sy–DNBA	I	130–320	38.62	38.81	DNBA
	II	320–600	41.50	41.43	$C_{12}H_{22}N_2O_2$
	Residue	–	19.48	19.76	9C
Sy–CLA	I	200–600	99.72	100.0	Sy+CLA

Sy–CLA. The observed shift in the ν(C–N) band upon complexation suggests that this group participated directly in the complexation. All these observations indicate the presence of hydrogen bonding in these complexes [39–44].

3.1.4. *^{1}H and ^{13}C NMR measurements*

The 600 MHz ^{1}H and ^{13}C NMR spectra of the synthesized salts were measured in DMSO-d_6 at room temperature. It has been found that the signal due to the phenolic proton (–OH) of the PA and DNBA acceptors, which is observed at δ ~11.94 ppm [45] and ~12.09 ppm [46] in the spectra of free PA and DNBA acceptors, respectively, is no longer observed. Instead, a new signal is observed at approximately ~6.45 ppm for PA complex and ~6.34 for DNBA complex. This singlet signal is assigned to the proton of the $^+$N–H species formed by the proton-transfer from the OH group of PA or DNBA to the nitrogen atom of the Sy [47]. This upfield shift in frequency has been attributed to an increase in π electron density on the PA or DNBA portion of the complex. The electronic environments of the Sy protons were affected by the presence of the (N^+–H) interaction. The singlet peak observed at 6.36 ppm in the Sy–CLA complex has been assigned to the $^+$N–H proton, while the singlet centered at 8.72 ppm is attributed to the non-hydrogen-bonded proton of the CLA moiety. Likewise, this peak is shifted slightly relative to the observed peak (at approximately δ~9.15 ppm) in the spectrum of free CLA [48]. Some changes are observed in the values of the chemical shifts of the Sy protons because of the presence of PT interactions between Sy and the acceptor molecules. The ^{13}C NMR spectrum of free Sy showed 20 resolved carbon signals (11 signals for *sp^3 carbons* and 9 signals for *sp^2 carbons*). In the ^{13}C NMR spectra of the products, the appearance of 25 (12 signals for *sp^3 carbons* and 13 signals for *sp^2 carbons*), 26 (12 signals for *sp^3 carbons* and 14 signals for *sp^2 carbons*) and 27 (12 signals for *sp^3 carbons* and 15 signals for *sp^2 carbons*) distinct

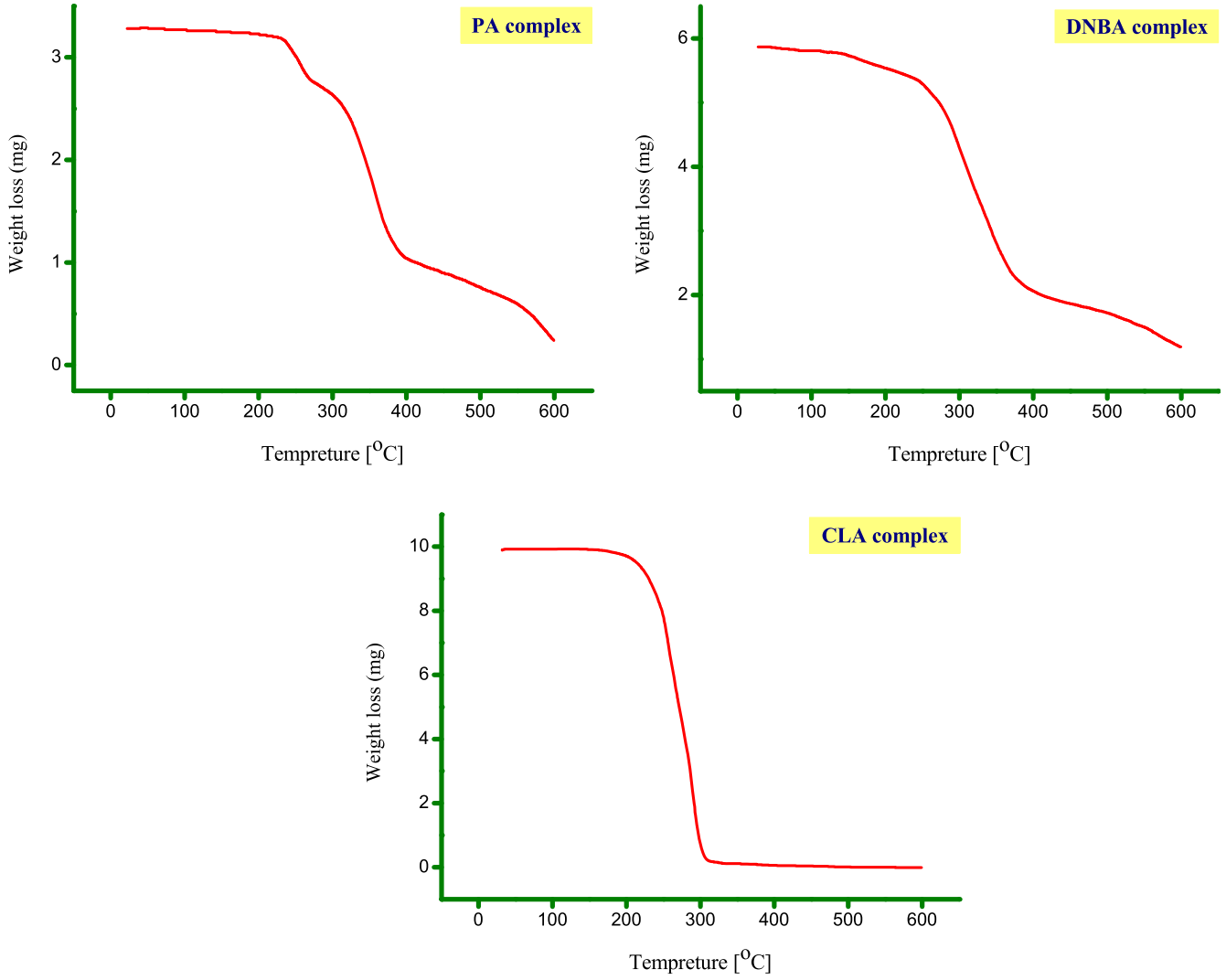

Fig. 10. TG thermograms plots of the Sy complexes with PA, DNBA and CLA acceptors.

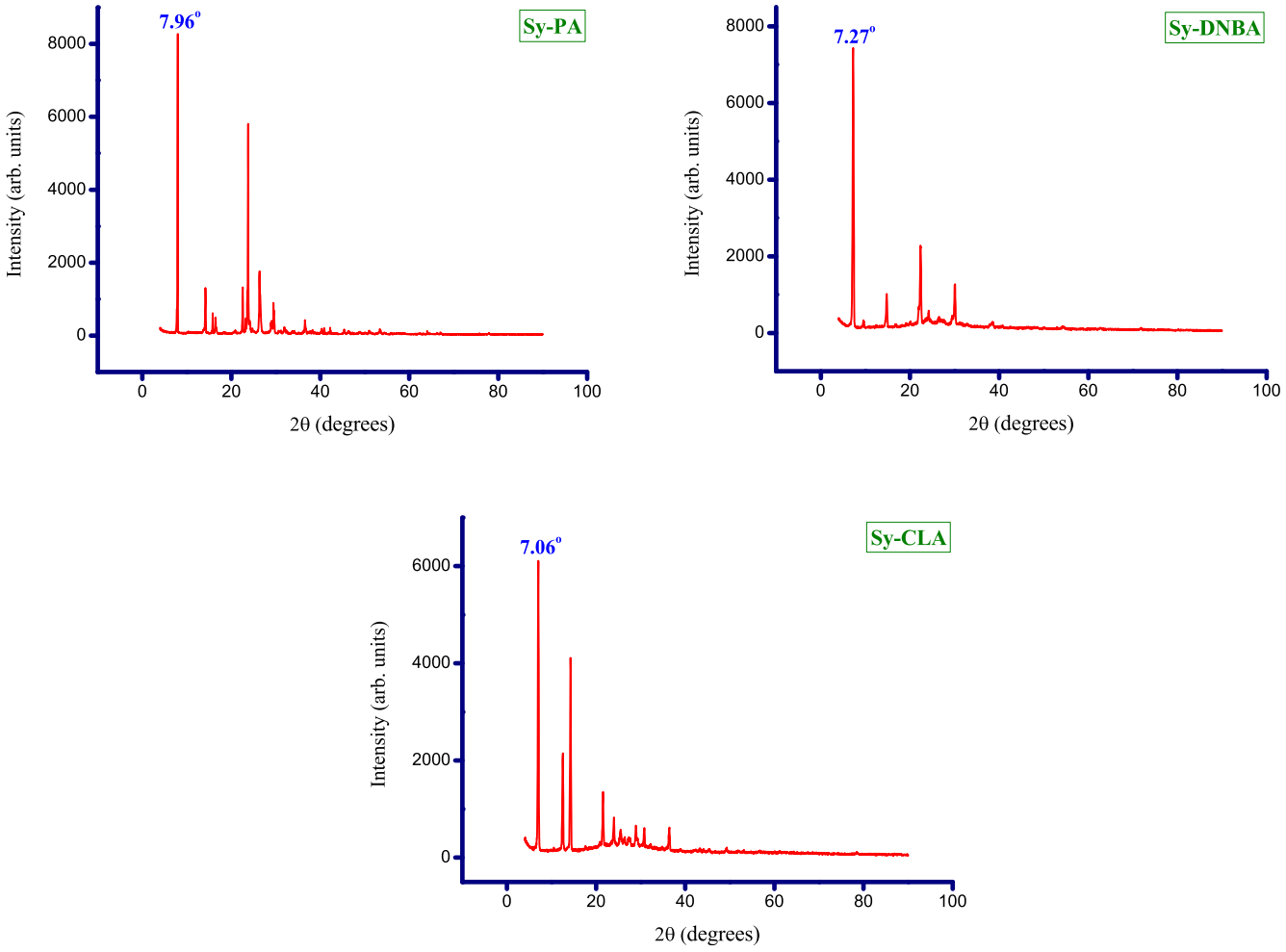

Fig. 11. XRD spectra of the Sy complexes with PA, DNBA and CLA acceptors.

resonant carbon signals in the spectra of the PA, DNBA and CLA complexes, respectively, is consistent with the proposed molecular structure of these complexes. For all complexes, common changes in the values of the ^{13}C chemical shifts in Sy can be observed as a result of its complexation with the organic acceptors. The structures of the synthesized complexes have been confirmed by IR, ^{1}H and ^{13}C NMR spectral data. The data obtained by these techniques are consistent with each other and support the predicted structures. Fig. 9 illustrates the proposed structures of the Sy complexes.

3.2. Thermal properties

3.2.1. Thermogram measurements

The thermal decomposition and stability of the synthesized salts were investigated by thermogravimetric (TG) analysis. The possible thermal degradation patterns for these salts are collected in Table 2, and their representative TG thermograms are depicted in Fig. 10. The TG thermogram of the Sy–PA complex indicated that this complex is decomposes in two degradation steps. The first decomposition step in the temperature range of 190–350 °C has a weight loss of approximately 40.84% and is attributed to the loss of the PA moiety. The final decomposition step occurred within the 350–600 °C temperature range corresponding to loss of $C_{17}H_{22}N_2O_2$ moiety representing a weight loss of (obs. = 50.32, cal. = 50.81%) then leaving residual carbon as final products. The complex containing the DNBA acceptor was thermally decomposed in nearly two decomposition steps within the 130–600 °C temperature range. The first stage of decomposition corresponds to the loss of acceptor molecule with a weight loss of 38.62%, which is in good agreement with the calculated value (38.81%). The second stage of decomposition corresponds to the removal of $C_{12}H_{22}N_2O_2$ moiety with a weight loss of 41.50% very close to the expected theoretical value of 41.43%. The final decomposition of the complex is the residual carbon atoms. The thermal degradation of the Sy–CLA complex occurs in one degradation stage. The complex begins decomposed at ~200 °C and was complete at ~600 °C, and

Table 3
XRD spectral data for the synthesized complexes.

Complex	2θ; (°)	θ; (°)	d-spacing value; (Å)	Height	β; FWHM	Particle size (nm)
Sy–PA	7.96	3.98	11.0981	7561.533	0.10	83
Sy–DNBA	7.27	3.64	12.1498	7368.619	0.29	25.6
Sy–CLA	7.06	3.53	12.5107	6178.710	0.05	166.2

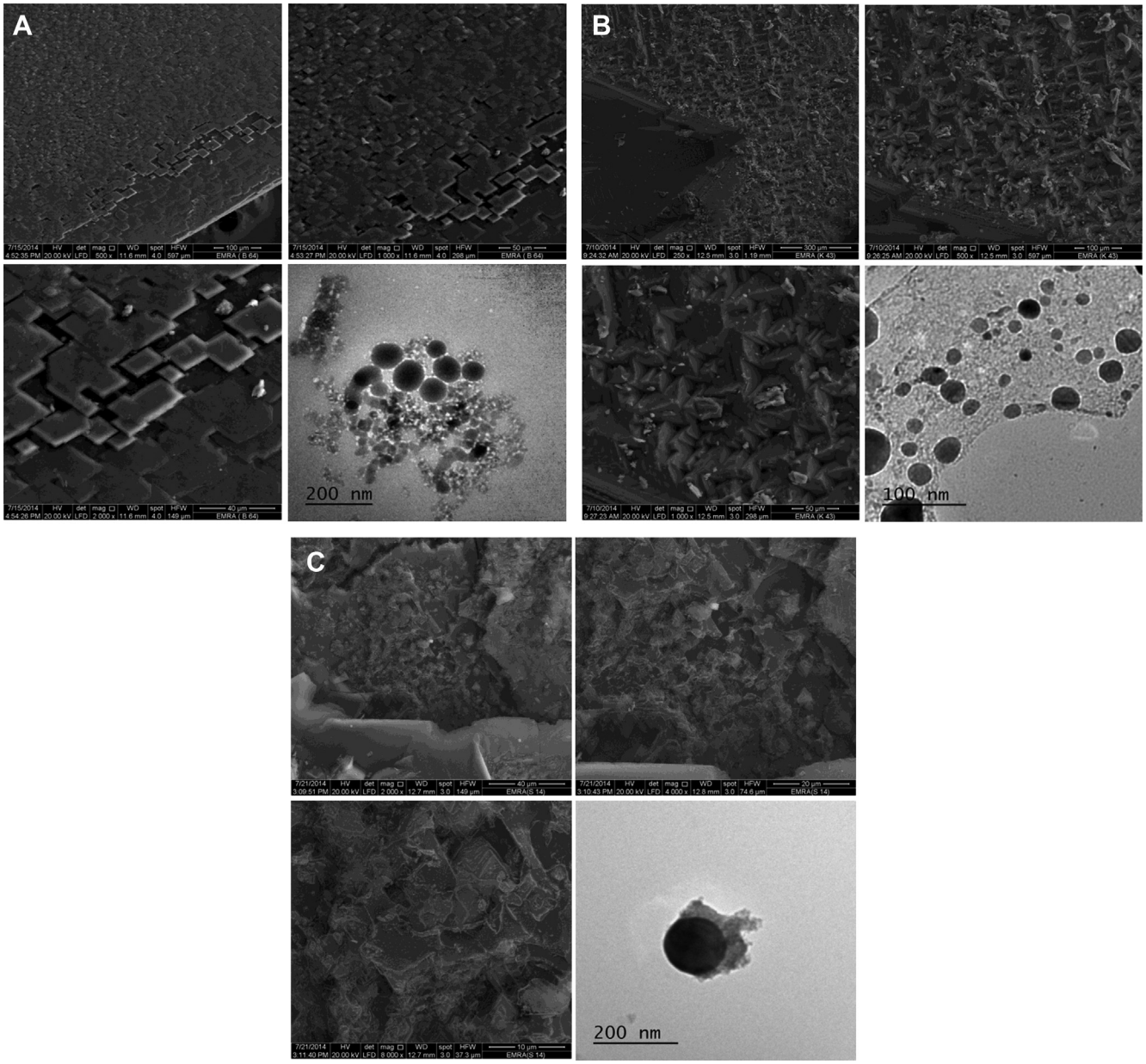

Fig. 12. (A). SEM and TEM images of the Sy–PA complex. (B). SEM and TEM images of the Sy–DNBA complex. (C). SEM and TEM images of the Sy–CLA complex.

the observed weight loss associated with this step is (obs. = 99.72, cal. = 100.0%), which can be attributed to the removal of the donor and acceptor moieties.

3.2.2. Comparison of the thermograms

The analyses of the TG thermograms of these salts provided the following observations:

i) The observed weight loss is in excellent agreement with the theoretical predictions.
ii) The Sy–CLA complex exhibited good thermal stability up to 200 °C.
iii) The complexes are stable up to ~190, 130 and 200 °C for Sy–PA, Sy–DNBA and Sy–CLA, respectively. Thus, these salts are stable in the solid state at room temperature and can be stored for several months without degradation.
iv) The CLA complex exhibit a one-stage degradation process.
v) The PA and DNBA complexes were thermally decomposed in approximately two decomposition steps.
vi) Generally, the first decomposition step is corresponded to the removal of the acceptor moiety.
vii) The decomposition in the second step is probable due to the donor removal.
viii) The decomposition of the CLA complex is almost complete without any carbon residue.
ix) The decomposition of PA and DNBA complexes led to residual carbon atoms as a final product.
x) The degradation data strongly support the formation of the synthesized salts and their proposed structures.

3.3. Structural properties

The surface morphology, nanometry, structural features and characteristics of the synthesized salts were observed by XRD, SEM

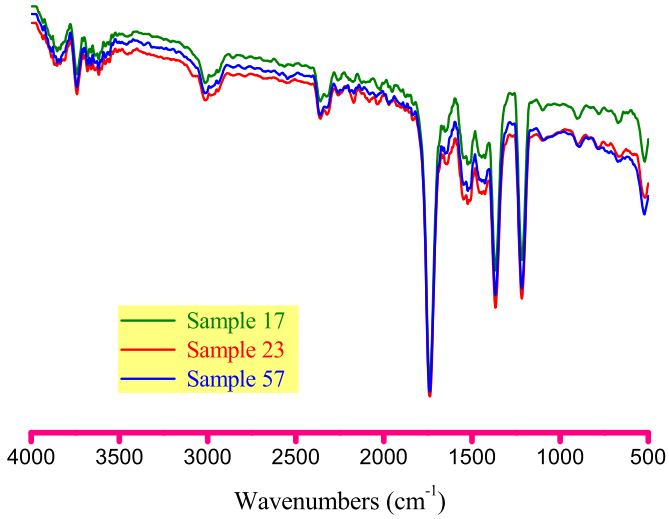

Fig. 13. IR spectra of the resultant carbon material samples.

and TEM analyses. Fig. 11 shows the indexed XRD patterns of the salts, and Table 3 presents the XRD spectral data for these salts. The strongest diffraction peak was observed at diffraction angles 2θ of 7.96°, 7.27°, and 7.06° for the Sy–PA, Sy–DNBA and Sy–CLA complexes, respectively. The appearance of a strong and narrow sharp diffraction peak indicated that the as-synthesized complex was well crystallized and has a well-defined structure. The particle size of these complexes was estimated from their XRD patterns based on the highest-intensity value using the well-known Debye–Scherrer formula. The calculated particle diameters of the Sy–PA, Sy–DNBA and Sy–CLA complexes were ~83, 26 and 166 nm, respectively, which are in good agreement with the results obtained by TEM. These values suggest that the particle sizes of the complexes are within the nanoscale range. Fig. 12(A, B and C) presents multiple SEM micrographs of the outer surfaces of the synthesized complexes at different levels of magnification (i.e., x500, x1000, x2000, x4000, x8000). The SEM micrographs of the particles revealed that all of the complexes have a well-defined shape, uniform matrix, distinct size and morphology with homogeneously dispersed nanoparticles, indicating the formation of homogeneous material. Visible morphological change is observed between the Sy complexes. From the high-quality and well-focused TEM micrographs (Fig. 12), it is inferred that all of the complexes are spherical nanoparticles that are homogeneously dispersed with no particle agglomeration. According to these micrographs, most of the nanoparticles of the Sy–PA, Sy–DNBA and Sy–CLA complexes exhibit diameters in the range of 54–90 nm, 10–30 nm and ~150 nm and main diameters of 72, 20 and 150 nm, respectively. We note that these diameters are in good agreement with the results calculated from the XRD data.

3.4. Characteristics of carbon materials

The as-prepared non-activated carbon products obtained from the direct carbonization of the Sy–PA (Sample 17), Sy–DNBA (Sample 23) and Sy–CLA (Sample 57) were ground into powder and characterized by IR, XRD, SEM and TEM techniques. Fig. 13 shows the IR spectra of the resultant carbon samples. The three samples exhibited similar IR spectra. In the these samples, the bands centered at 1000–1300 cm^{-1} are related to the C–OH stretching

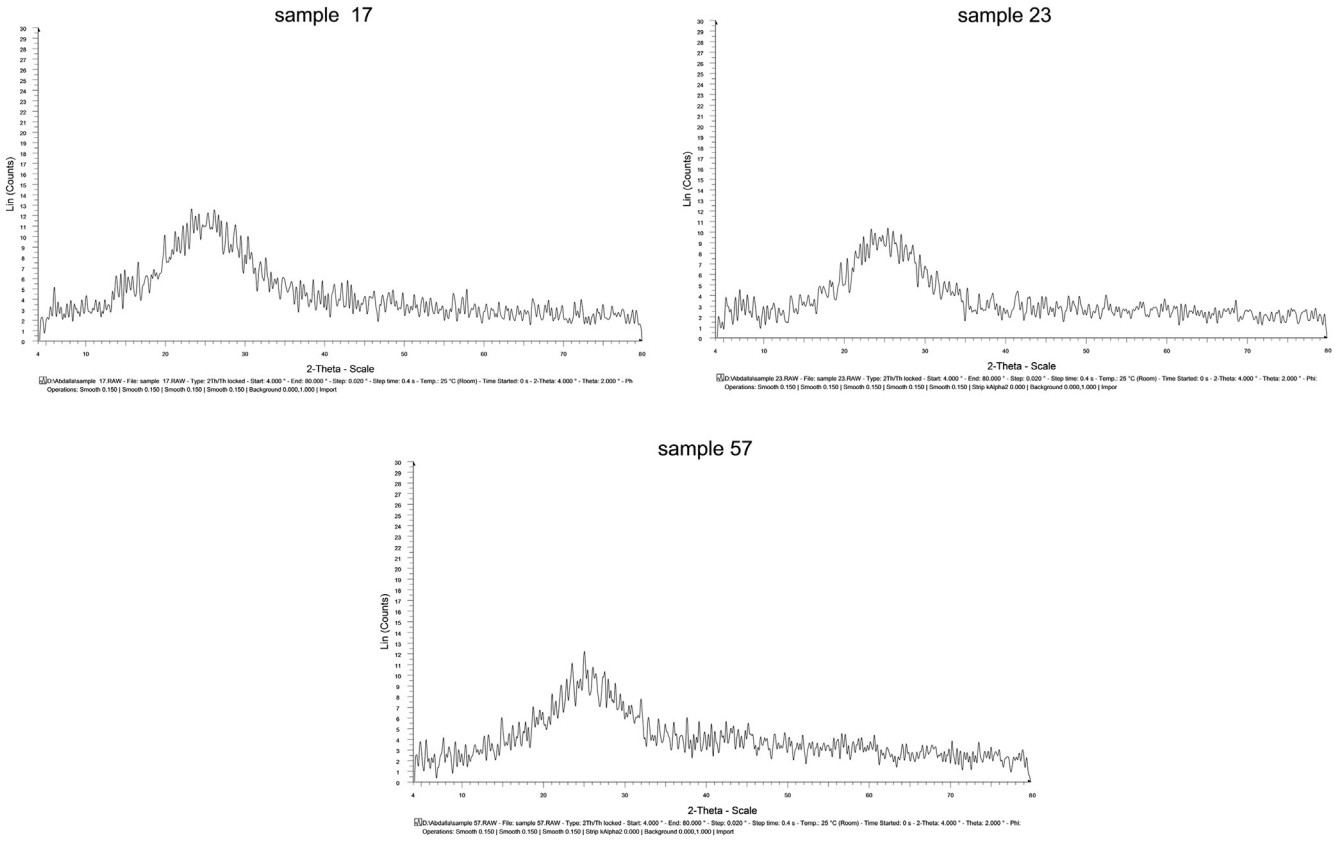

Fig. 14. XRD spectra of the resultant carbon material samples.

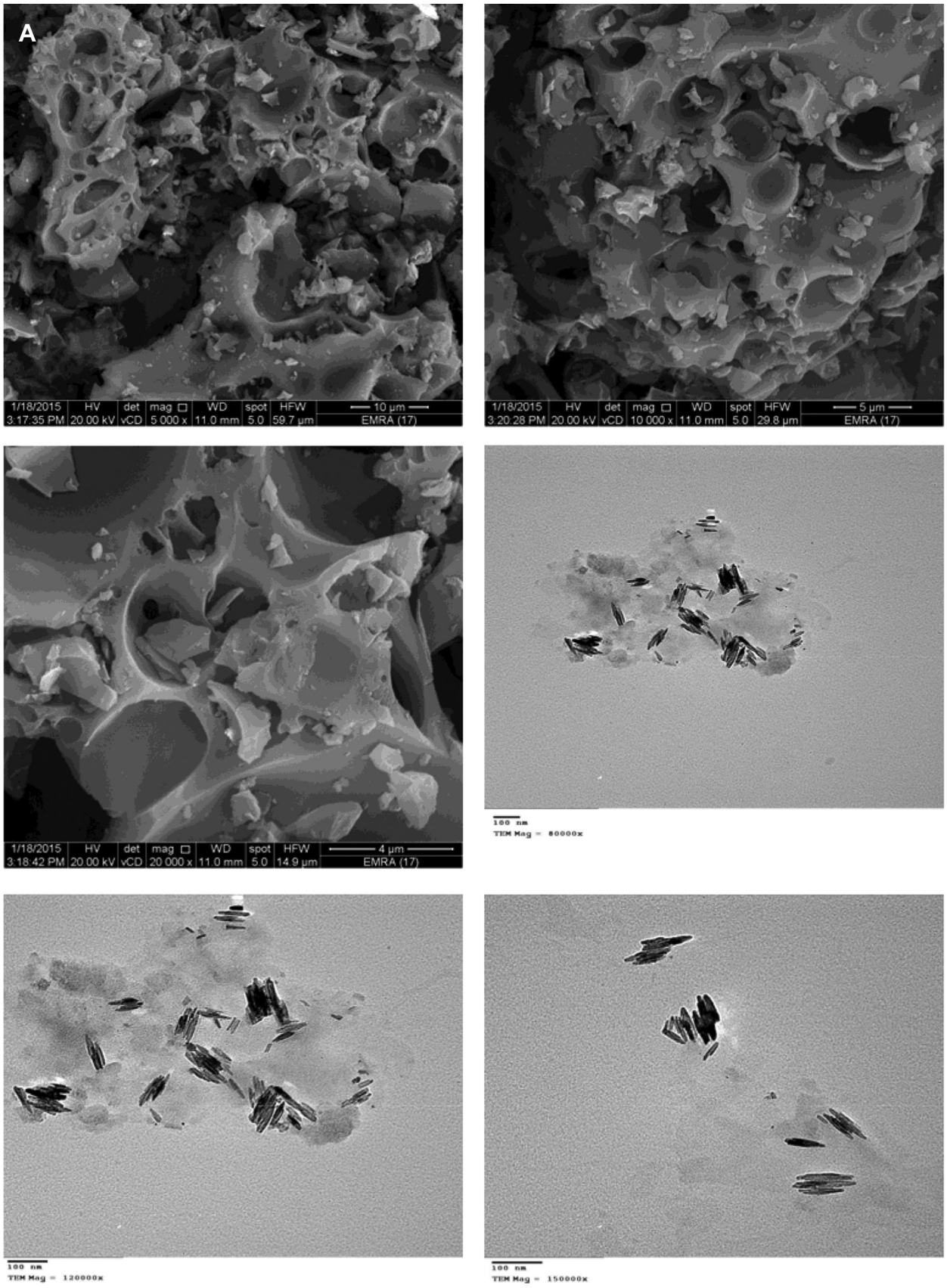

Fig. 15. (A). SEM and TEM images of carbon product obtained by the carbonization of Sy–PA complex; Sample 17. (B). SEM and TEM images of carbon product obtained by the carbonization of Sy–DNBA complex; Sample 23. (C). SEM and TEM images of carbon product obtained by the carbonization of Sy–CLA complex; Sample 57.

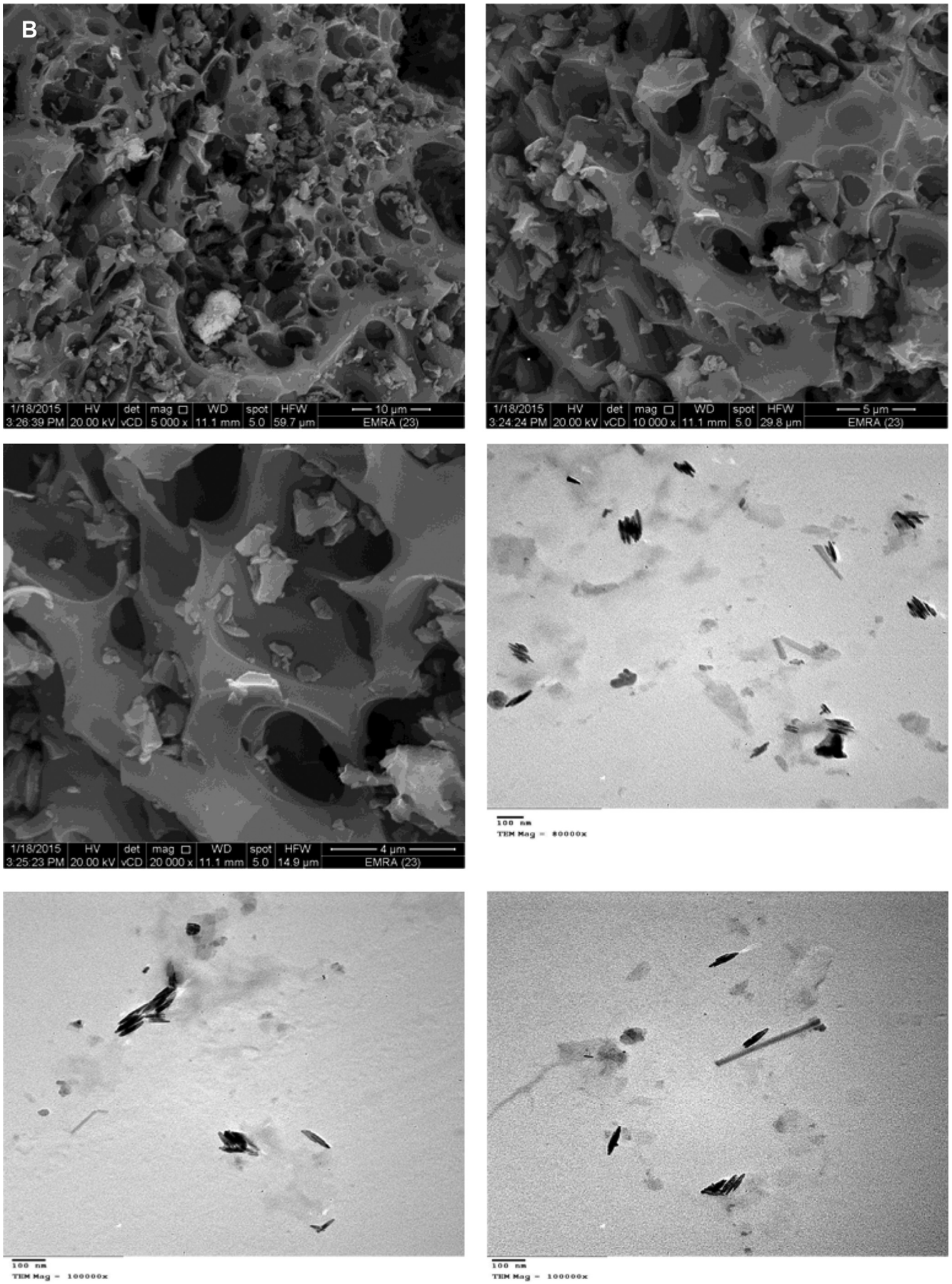

Fig. 15. (*continued*).

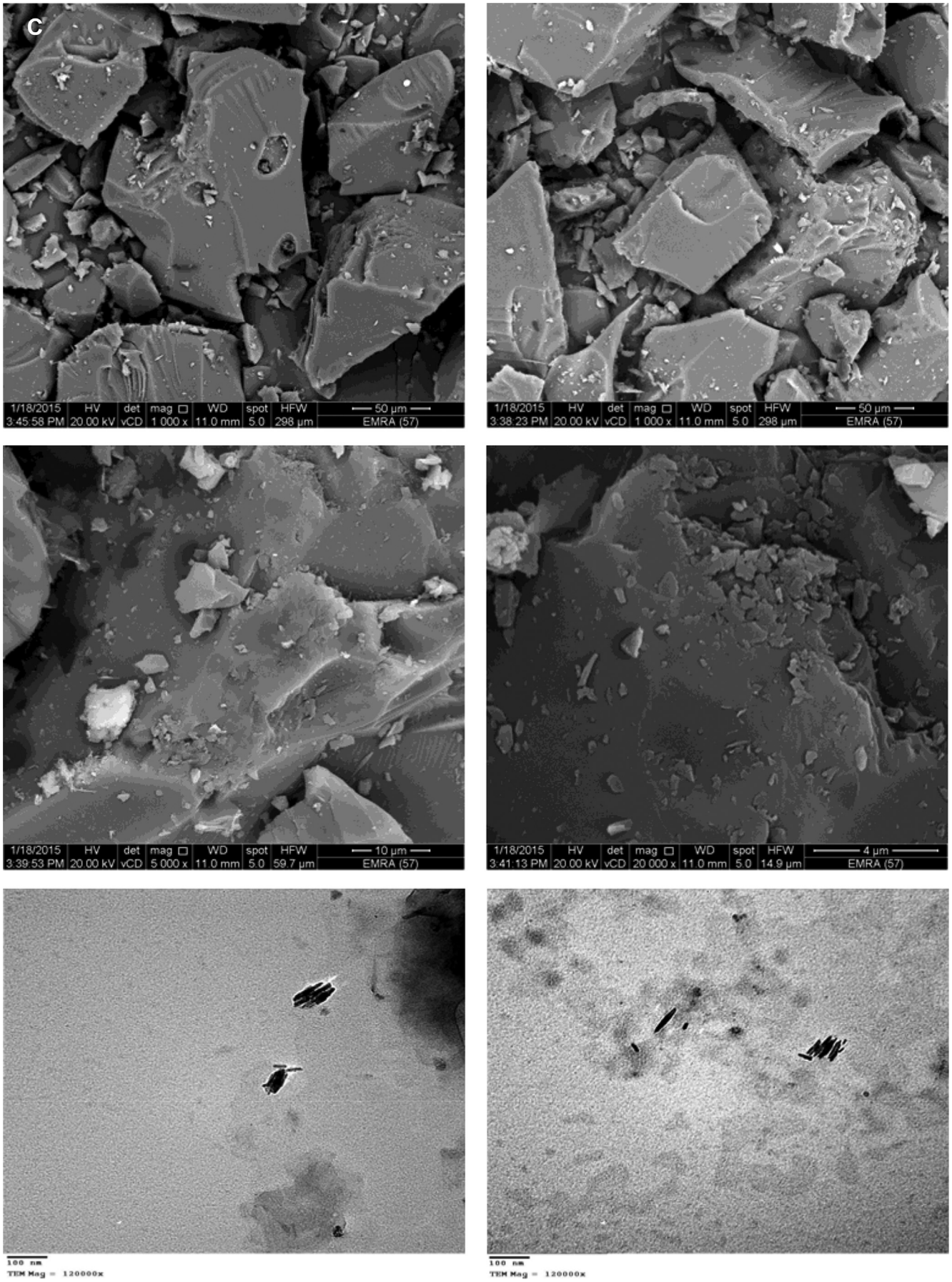

Fig. 15. (*continued*).

vibration and –OH bending vibration [49]. The band 1730 cm^{-1} could be ascribed to C=O stretching vibration, and the other adsorption bands at 1400–1500 cm^{-1} and 2900–3020 cm^{-1} correspond to the C–H bending vibration and stretching vibration, respectively [50]. The absorptions at around 3600 cm^{-1} could be attributed to O–H stretching vibration and the strong band around 1215 cm^{-1} could be assigned to the C–N stretching vibration. Thus, the IR analysis confirms the existence of oxygen-, nitrogen- and hydrogen-containing functional groups in the carbon samples. To confirm the framework structure of materials, XRD patterns of resultant carbons were characterized and shown in Fig. 14. The three samples exhibited similar XRD patterns. The profiles of these samples displayed one broad peak located at a 2θ of approximately 25°. It matches well with the profiles previously reported [51–53] for non-graphitic carbon. The absence of a sharp diffraction pattern indicated that the resulting porous carbon mainly possesses an amorphous structure [54,55]. Furthermore, no impurity diffraction was observed, confirming the absence of any other x-ray traceable compounds in the carbon product. To reveal the morphology of all carbon materials and investigate the influence of acceptor molecule on the morphology, SEM and TEM images of all carbon products are shown in Fig. 15(A, B and C). The multiple SEM micrographs at different degrees of enlargement (i.e., x5000, x10000, x20000) indicate the carbons have uniform morphology. We surprisingly found that the complexation of Sy with the PA or DNBA acceptor leads to a well-developed porosity carbon material, while its complexation with CLA acceptor forms non-porous carbon product. The highly magnified (x80000–150000) TEM micrographs show that the length of the carbon particles is approximately 100 nm. The XRD, SEM and TEM analyses confirm that the direct carbonization of the PA and DNBA complexes leads to nanoporous carbon material.

4. Conclusions

A method was proposed to remove and utilize strychnine (Sy) based on complexation with acido organic acceptors (PA, DNBA and CLA) followed by direct carbonization of the resultant salts into carbon materials. The structure, spectroscopic properties and morphology of the products were fully characterized by using physicochemical and spectroscopic techniques, such as UV–visible, IR, ^{1}H NMR and ^{13}C NMR spectroscopies; XRD; SEM; TEM; and elemental analysis. The results indicate that all salts are formed based on a 1:1 stoichiometric ratio. The IR, ^{1}H and ^{13}C NMR spectra of the products clearly indicate the formation of the complexes. Our findings indicated that the paired molecules in the Sy–PA and Sy–DNBA and Sy–CLA are linked by intermolecular hydrogen-bonding interactions. The proposed method is simple, environmentally friendliness, direct without complicates procedures and can be generally used in preparation of porous and non-porous carbons.

Conflict of interests

The authors declare no financial/commercial conflict of interests regarding the study.

References

[1] R. Bhati, A. Singh, V.A. Saharan, V. Ram, A. Bhandari, J. Ayurveda Integr. Med. 3 (2) (2012) 80–84.
[2] F. Liu, X. Wang, X. Han, X. Tan, W. Kang, Int. J. Biol. Macromol. 77 (2015) 92–98.
[3] A. Rathi, N. Srivastava, S. Khatoon, A.K.S. Rawat, Chromatographia 67 (2008) 607–613.
[4] E.P. Marques, F. Gli, P. Proenca, P. Monsanto, M.F. Oliveira, A. Castanheira, D.N. Vieira, Forensic Sci. Int. 110 (2000) 145–152.
[5] X.H. Zang, C.R. Li, Q.H. Wu, C. Wang, D.D. Han, Z. Wang, Chin. Chem. Lett. 18 (2007) 316–318.
[6] A.J. Duke, Handbook of Medicinal Plants, vol. 20, Coordinating Research Council Press, Boca Raton, Florida, 1985, pp. 34–35.
[7] G. Philippe, L. Angenot, M. Tits, M. Frédérich, Toxicon 44 (2004) 405.
[8] L. Yu, Q. Xu, Y. Yu-Wei, P. Yang, B. Hui-Min, Chin. J. Nat. Med. 12 (10) (2014) 760–767.
[9] S. Kodikara, J. Forensic Leg. Med. 19 (2012) 40–41.
[10] Y.P. Zhai, Y.Q. Dou, D.Y. Zhao, P.F. Fulvio, R.T. Mayes, S. Dai, Adv. Mater 23 (2011) 4828–4850.
[11] I.I. Zhang, X.S. Zhao, Chem. Soc. Rev. 38 (2009) 2520–2531.
[12] M. Inagakia, H. Konno, O. Tanaike, J. Power Sources 195 (2010) 7880–7903.
[13] J. Zhu, J. Cheng, A. Dailly, M. Cai, M. Beckner, P. Shen, Int. J. Hydrogen Energy 39 (2014) 14843–14850.
[14] M.S. Refat, H.A. Saad, A.M.A. Adam, Spectrochim. Acta A 141 (2015) 202–210.
[15] M.S. Refat, L.A. Ismail, A.M.A. Adam, Spectrochim. Acta A 134 (2015) 288–301.
[16] M.S. Refat, A.M.A. Adam, H.A. Saad, J. Mol. Strut. 1085 (2015) 178–190.
[17] A.M.A. Adam, M.S. Refat, J. Mol. Liq. 209 (2015) 33–41.
[18] A.M.A. Adam, Russ. J. Gen. Chem. 84 (6) (2014) 1225–1236.
[19] A.M.A. Adam, M.S. Refat, Russ. J. Gen. Chem. 84 (9) (2014) 1847–1856.
[20] A.M.A. Adam, Spectrochim. Acta A 127 (2014) 107–114.
[21] M.S. Refat, O.B. Ibrahim, H.A. Saad, A.M.A. Adam, J. Mol. Struct. 1064 (2014) 58–69.
[22] M.S. Refat, A.M.A. Adam, J. Mol. Liq. 196 (2014) 142–152.
[23] M.S. Refat, A.A. Gobouri, A.M.A. Adam, H.A. Saad, Phys. Chem. Liqs. 52 (5) (2014) 680–696.
[24] A.M.A. Adam, Spectrochim. Acta A 104 (2013) 1–13.
[25] A.M.A. Adam, M.S. Refat, H.A. Saad, J. Mol. Strut. 1051 (2013) 144–163.
[26] A.M.A. Adam, M.S. Refat, H.A. Saad, J. Mol. Strut. 1037 (2013) 376–392.
[27] A.M.A. Adam, M.S. Refat, T. Sharshar, Z.K. Heiba, Spectrochim. Acta A 95 (2012) 458–477.
[28] A.M.A. Adam, J. Mol. Struct. 1030 (2012) 26–39.
[29] H.A. Benesi, J.H. Hildebrand, J. Am. Chem. Soc. 71 (1949) 2703–2707.
[30] G. Briegleb, Z. Angew. Chem. 76 (1964) 326–341.
[31] H. Tsubomura, R.P. Lang, J. Am. Chem. Soc. 83 (1961) 2085–2092.
[32] R. Rathone, S.V. Lindeman, J.K. Kochi, J. Am. Chem. Soc. 119 (1997) 9393–9404.
[33] G.G. Aloisi, S. Pignataro, J. Chem. Soc. Faraday Trans. 69 (1973) 534–539.
[34] M.A. Estermann, W.I.F. David, in: W.I.F. David, K. Shankland, I.B. Mccusker, Ch Baerlocher (Eds.), Structure Determination from Powder Diffraction Data (SDPD), Oxford Science Publications, New York (, 2002.
[35] D.A. Skoog, Principle of Instrumental Analysis, third ed., Saunders, New York, USA, 1985 [Chapter 7].
[36] N. Islam, S. Niaz, T. Manzoor, A.H. Pandith, Spectrochim. Acta A 131 (2014) 461–470.
[37] V.A. Narayanan, N.A. Stump, G.D. Del Cul, T. Vo-Dinh, J. Raman Spectrosc. 30 (1999) 435–439.
[38] M. Manikandan, T. Mahalingam, Y. Hayakawa, G. Ravi, Spectrochim. Acta A 101 (2013) 178–183.
[39] N. Singh, A. Ahmad, J. Mol. Strut. 1074 (2014) 408–415.
[40] E. Selvakumar, G. Anandha babu, P. Ramasamy, A. Chandramohan, Spectrochim. Acta A 122 (2014) 436–440.
[41] M.Y. El-Sayed, M.S. Refat, Spectrochim. Acta A 137 (2015) 1270–1279.
[42] N. Singh, I.M. Khan, A. Ahmad, S. Javed, J. Mol. Liq. 191 (2014) 142–150.
[43] N. Singh, I.M. Kahn, A. Ahmed, S. Javed, Mol. Struct. 1065–1066 (2014) 74–85.
[44] X. Ding, Y. Li, S. Wang, X. Li, W. Huang, J. Mol. Struct. 1062 (2014) 61–67.
[45] R. Bharathikannan, A. Chandramohan, M.A. Kandhaswamy, J. Chandrasekaran, R. Renganathan, V. Kandavelu, Cryst. Res. Technol. 43 (2008) 683–688.
[46] N. Singh, I.M. Khan, A. Ahamd, S. Javed, J. Mol. Strut. 1066 (2014) 74–85.
[47] A.A. Rzokee, A. Ahmad, J. Mol. Struct. 1076 (2014) 453–460.
[48] A.S. AL-Attas, M.M. Habeeb, D.S. AL-Raimi, J. Mol. Struct. 928 (2009) 158.
[49] R. Demir-Cakan, N. Baccile, M. Antonietti, M.M. Titirici, Chem. Mater 21 (2009) 484–490.
[50] S. Ikeda, K. Tachi, Y.H. Ng, Y. Ikoma, T. Sakata, H. Mori, T. Harada, M. Matsumura, Chem. Mater 19 (2007) 4335–4340.
[51] X. Yan, X. Li, Z. Yan, S. Komarnei, Appl. Surf. Sci. 308 (2014) 306–310.
[52] J. Zhu, J. Cheng, A. Dailly, M. Cai, M. Beckner, P. Shen, Int. J. Hydrogen Energy 39 (2014) 14843–14850.
[53] Y. Xiao, H. Chen, M. Zheng, H. Dong, B. Lei, Y. Liu, Mater. Lett. 116 (2014) 185–187.
[54] M. Okamura, A. Takagaki, M. Toda, J.N. Kondo, T. Tatsumi, K. Domen, M. Hara, S. Hayashi, Chem. Mater 18 (2006) 3039–3045.
[55] B.H. Zhang, J.W. Ren, X.H. Liu, Y. Guo, Y.L. Guo, G.Z. Lu, Y.Q. Wang, Catal. Commun. 11 (2010) 629–632.